Benchmarking of Full-F Global Gyrokinetic Modeling Results Against the FT-2 Tokamak Doppler Reflectometry Data Using Synthetic Diagnostics

A Altukhov, A Gurchenko, E Gusakov, M Irzak, O Krutkin, L Esipov, P Niskala, T Kiviniemi, S Leerink, C. Lechte, et al.

BENCHMARKING OF FULL-F GLOBAL GYROKINETIC MODELING RESULTS AGAINST THE FT-2 TOKAMAK DOPPLER REFLECTOMETRY DATA USING SYNTHETIC DIAGNOSTICS

A.B. ALTUKHOV, A.D. GURCHENKO, E.Z. GUSAKOV, M.A. IRZAK, O.L. KRUTKIN, L.A. ESIPOV
Ioffe Institute
St. Petersburg, Russia
Email: a.altuhov@mail.ioffe.ru

P. NISKALA, T.P. KIVINIEMI, S. LEERINK
Aalto University
Espoo, Finland

C. LECHTE
Institute of Interfacial Process Eng. and Plasma Technology
70569 Stuttgart, Germany

S. HEURAUX
Institute Jean Lamour UMR 7198 CNRS, Université de Lorraine
54000 Nancy, France

Abstract

Two versions of the X-mode Doppler reflectometry (DR) synthetic diagnostics are developed in the framework of the ELMFIRE global GK modeling of the FT-2 tokamak ohmic discharge. In the "fast" version DR signal is computed in the linear theory approximation using the reciprocity theorem utilizing the probing wave field pattern provided by computation taking into account the 2D plasma inhomogeneity effects, whereas the alternative "slow" version of DR synthetic diagnostic is based on the full-wave code IPF-FD3D describing the probing and scattered wave propagation in turbulent plasma. The DR signal frequency spectra and the dependence of their frequency shift, width and shape on the probing antenna position are computed and shown to be similar to those measured in the high field side probing DR experiment at the FT-2 tokamak. The GAM characteristics provided by the measurements and by the synthetic DR are close within a 12% accuracy. However the variation of the DR signal at growing incidence angles in experiment is slower than predicted by both synthetic diagnostics. The substantial difference was found also in the decay of the DR signal CCFs with growing frequency shift in the probing wave channels. The quick decrease of the RCDR coherence observed in the experiment and full-wave synthetic diagnostic compared to the fast synthetic RCDR is attributed to the phase modulation of the probing wave in the former two cases due to the long-scale density fluctuations, which is shown to be close to $\pi/4$ both in the specially performed measurements and in the GK modelling. In spite of the fact that this value indicates only the beginning of the transition to the fluctuation reflectometry nonlinear regime, which therefore is not influencing the DR spectra, it already has a strong influence on the RCDR performance.

1. INTRODUCTION

The anomalous energy transport remains the main unresolved enigma on the way to the realisation of magnetic confinement fusion using the tokamak concept. According to the present day understanding [1, 2] the anomalous transport is determined by the multi-scale drift-wave turbulence and is strongly dependent on the nonlinear interaction of its components, such as large-scale mean E×B flows, meso-scale zonal flows and fine-scale micro-turbulence excited due to specific profiles of plasma parameters. That interaction controlling the anomalous transport has been in the focus of theoretical and experimental research in magnetically confined plasmas for a long time. The massively parallelized particle-in-cell simulations of the gyrokinetic (GK) distribution function and the electric field [3, 4] provide an efficient theoretical tool for studying the nonlinear turbulent plasma dynamics, which, however, needs a validation and comprehensive benchmarking against the experimental data. In the recent papers [5, 6] such simulations of the electron and ion distribution function from the first principles were performed for the small research limiter tokamak FT-2 [4]. The complex interplay of the multi-scale turbulence components was studied in simulations and successful quantitative comparison was presented with measurements carried out at the low magnetic field side of the machine with O-mode Doppler reflectometry and enhanced microwave scattering in the upper hybrid resonance [5, 6].
In the present paper the results of the global GK particle-in-cell simulations will be quantitatively compared to the X-mode Doppler reflectometry experimental data obtained at the high magnetic field side of the FT-2 tokamak (these data characterize the tokamak turbulent dynamics and transport phenomena at micro, macro and meso-scale). Doppler reflectometry (DR) is the microwave diagnostic widely used nowadays in toroidal fusion

experiments to get information on the multi-scale anomalous transport phenomena — namely, on plasma rotation at ASDEX UG (the mean value and its oscillations) [7] and turbulence poloidal wavenumber spectrum at Tore Supra [8]. Just recently the radial correlation modification of this technique proposed at ASDEX UG [9] providing information on the turbulence radial structure was justified [10, 11]. Unfortunately, the interpretation of DR data is complicated by the contribution of the poorly localized small-angle scattering along the wave trajectory, which can lead to the overestimation of the turbulence radial correlation length in the linear scattering regime, and to its underestimation in the strongly nonlinear regime. In the latter case the turbulence wavenumber spectrum measurements are questionable, and only the plasma turbulence mean velocity could be determined (however, with poor spatial resolution) [12]. Moreover, in the case of X-mode DR the turning point can not be determined unambiguously due to the 2D propagation effects, which additionally complicates the experimental data interpretation and its comparison with the theory predictions. Development of a synthetic diagnostics, allowing the direct signal computation based on the results of GK modeling, could be helpful in this case both for the interpretation of the experimental results and for the code benchmarking. In this paper two versions of the X-mode DR synthetic diagnostics are developed in the framework of the ELMFIRE global GK modeling of the FT-2 tokamak ohmic discharge [6]. The X-mode DR signal is computed both in the linear theory approximation using the reciprocity theorem utilizing the probing wave field pattern provided by computation taking into account the 2D plasma inhomogeneity effects [13] and by the full-wave code IPF-FD3D describing the probing and scattered wave propagation in turbulent plasma [14]. The temporal behavior of the DR signal frequency spectra and the dependence of its amplitude, frequency shift and shape on the probing antenna position are computed and compared to those measured in the experiment at the FT-2 tokamak. In the case of multi-frequency probing the radial correlation (RC) DR cross-correlation function (CCF) is also determined by both synthetic diagnostics and compared to that obtained in the experiment. The role of probing wave phase modulation in performance of RCDR is investigated both in computations and experimentally.

2. THE EXPERIMENTAL APPROACH.

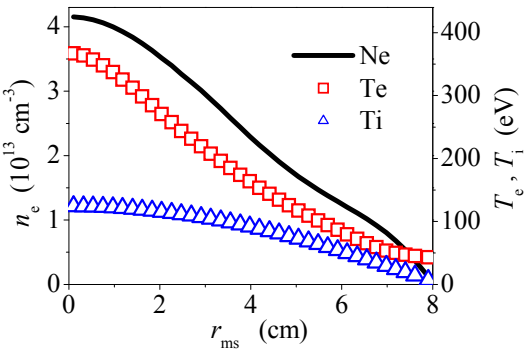

FIG.1. The discharge parameter profiles. Density – solid curve; electron temperature – squares; ion temperature – triangles.

The experiment was performed at the FT-2 tokamak (a major radius $R = 55$ cm, limiter radius $a = 7.9$ cm) in the hydrogen ohmic discharge (with plasma current $I_p = 19$ kA, central density $n_e(0) = 4\times10^{13}$ cm^{-3} and electron temperature $T_e = 470$ eV). The discharge is similar to that utilized for successful comprehensive benchmarking of the ELMFIRE GK code in [5, 6], however, the toroidal magnetic field at the discharge axis is slightly smaller ($B_t(0) = 1.7$ T instead of 2.1 T). The actual measured electron density and temperature profiles for this discharge used in the GK modelling, as well as the ion temperature profile are shown in Fig. 1. The vertically movable (by ±2 cm) X-mode double antenna set (shown in Fig.2) installed at high magnetic field side in equatorial plane allowed plasma probing at variable incidence angle with frequencies in the range $f_i = (50\text{-}75)$ GHz. It was used both in standard DR measurements utilizing the quadrature scheme and in the RCDR technique based on the scheme described in [15]. In the former case the DR spectrum was obtained via averaging of 155 random DR power spectra obtained by using Fourier transform of 12.8 microsecond samples of the DR signal. In the latter case the reference channel generator was tuned to the master frequency $f_0 = 70$ GHz determining the measurement position in the vicinity of $r = 5$ cm, whereas another generator producing probing signal at a slave frequency varied in the interval [1.2; 1.2] GHz around the master frequency in 100 MHz steps was used in the second, (signal), channel to determine the turbulence two-point CCF.

The backscattering (BS) spectra $P_s(f_s - f_i) \equiv P_s(f)$ (f_i and f_s are probing and scattering frequencies accordingly) measured by the X-mode DR diagnostics at different vertical antenna displacements were presented in [12, 12A]. It was shown there that the BS power is decreasing with growing antenna vertical shift corresponding to increase of the probing wave incidence angle, whereas the spectra frequency shifts and width are increasing.

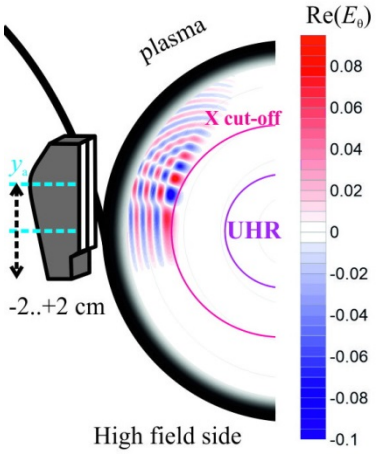

FIG.2. The DR experiment geometry and the probing wave poloidal electric field distribution computed at y_a=1.5 cm.

3. THE GK COMPUTATION APPROACH AND THE SYNTHETIC DIAGNOSTICS.

The simulations are performed with the global electrostatic particle-in-cell code ELMFIRE [3] to model the evolution of the full distribution function of drift kinetic electrons and gyrokinetic protons and O^{6+} ions. The simulation geometry has a circular cross-section and covers all the radial range. The time step is set to $\delta t = 30$ ns and spatial grid to 110×515×8 cells in radial (r), poloidal (θ), and toroidal (φ) direction. Approximately 2400 electrons and ions are simulated per grid cell. Momentum and energy conserving binary collision operator [16] is applied allowing the inclusion of neoclassical physics in the simulations.
The particles are initialized according to a prescribed temperature and density profiles taken close to the experimentally measured ones (see Fig.1). The profiles are allowed to develop self-consistently in time, while turbulence develops and heat sources and sinks, namely Ohmic heating and radiation losses, are applied. The Ohmic heating is induced by a spatially homogeneous loop voltage [17, 18], while electrons are cooled using a Monte Carlo model according to an impurity radiation loss distribution measured by the bolometry diagnostics. The initial oxygen O^{6+} impurity density is chosen in order to provide the experimental value of $Z_{\text{eff}} = 2.2$, as determined using ASTRA modeling and experimental loop voltage measurements, with equal temperatures for the impurities and main ions. Neumann and Dirichlet boundary conditions are used at the inner and outer boundary of the simulation geometry for the electrostatic potential. Particles passing the inner boundary are reflected back into the simulation domain whereas particles passing the outer boundary are returned to the simulation domain as an electron-ion pair according to a probability distribution proportional to the measured radial profile of neutral hydrogen density and at the wall temperature.
The fast synthetic X-mode DR diagnostics developed for this code [13] is based on the reciprocity theorem of electrodynamics [19] relating the high-frequency current in the plasma volume and the signal radiated by it and received by the antenna. The probing and backscattering wave propagation in the plasma not perturbed by turbulence is described in the fast synthetic diagnostic by full-wave code WaveTOP2D [20]. The code solves complete Maxwell equations in toroidal geometry accounting for the magnetic field shearing. Turbulent density fluctuations computed in the eight toroidal cross-sections were used to obtain the DR signal lasting 0.96 ms. This realization was divided into 0.012 ms samples in which the random Fourier spectra were calculated later used to obtain the average DR spectrum. It should be mentioned however that the approach based on the reciprocity theorem neglects the perturbations of the probing wave propagation caused by the density fluctuations, in particular, multiple small-angle scattering or its strong phase modulation. In this sense it is equivalent to the so called Born approximation linear in the fluctuation amplitude. The main merit of this approach is the possibility of fast computations, whereas the main drawback is related to the neglecting the nonlinear effects.
The alternative "slow" DR synthetic diagnostic is free from this drawback. It is based on the full-wave code IPF-FD3D describing the probing and scattered wave propagation in turbulent plasma [14] It is accounting for perturbations introduced by density fluctuations and therefore is not limitted to the linear approximation, however solves Maxvell equations for a single mode in the case of propagation perpendicular to the magnetic fieild and neglecting its poloidal component and toroidicity.

4. DR FREQUENCY SPECTRA COMPARISON

The DR spectra obtained in the experiment and provided by synthetic diagnostics are compared in Fig. 3 for vertical antenna shifts of different sign.
As it is seen in the figures, spectra provided by both synthetic diagnostics fit reasonably well the experimental ones for all the antenna positions. Not only are the shifts of both spectra close in all cases, but their shapes also look alike. This impression is confirmed in Fig. 4 and Fig. 5, where the mean frequency shift

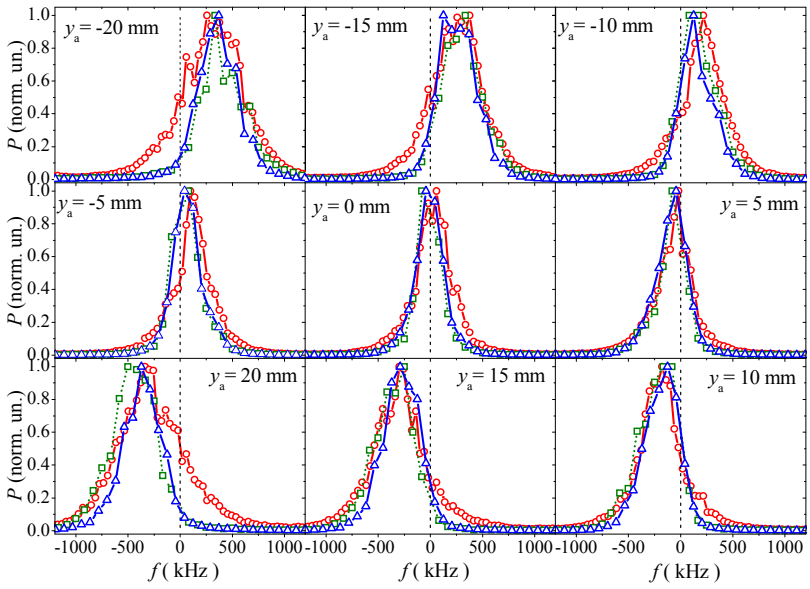

FIG.3 Comparison of DR spectra for different antenna vertical displacement. Circles – experiment; triangles – fast synthetic DR, squares – full-wave synthetic DR.

$f_D = \int f \cdot P_s(f)df \Big/ \int P_s(f)df$ and mean frequency width $\Delta f = \left[\int (f - f_D)^2 \cdot P_s(f)df \Big/ \int P_s(f)df \right]^{1/2}$ of the experimental and synthetic spectra obtained as the first and the second moment of the spectrum accordingly are plotted as functions of the antenna vertical displacement and the turbulence poloidal wavenumber.

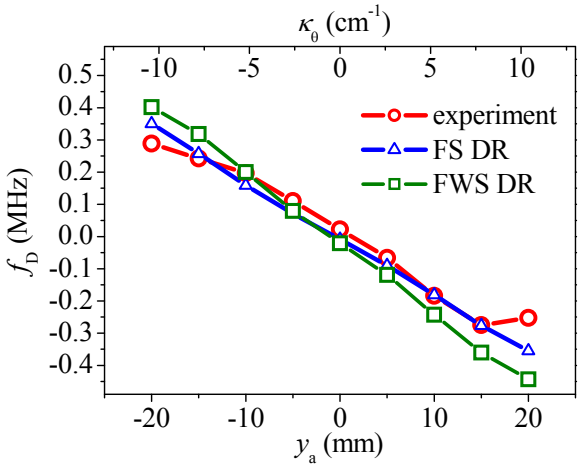

FIG. 4 Dependence of the DR signal frequency shift on the antenna vertical displacement y_a and fluctuation wavenumber. Circles –experiment; triangles – fast synthetic DR; squares full-wave synthetic DR.

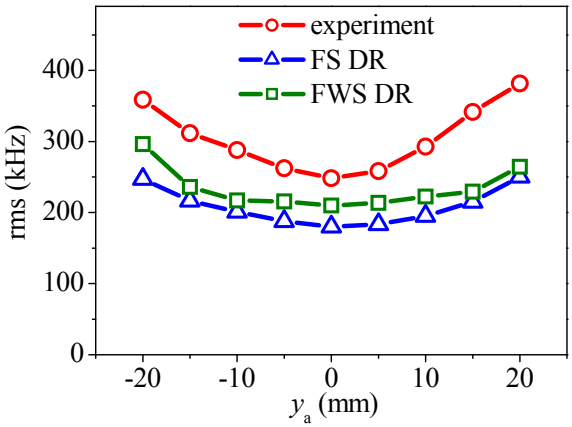

FIG. 5 Dependence of the DR signal frequency width (rms) on the antenna vertical displacement y_a. Circles –experiment; triangles – synthetic DR.

The relation between the antenna displacement and the fluctuation poloidal wavenumber was obtained using the X-mode ray-tracing (the doubled value of the probing wave poloidal wavenumber at the trajectory minimal radial coordinate). The spectral shift data provided by the experiment and GK modeling agree surprisingly well. The meaningful difference is only observed at the largest antenna displacement $y_a = \pm 2.0$ cm. This difference is probably due to a contribution of experimental spectrum tails becoming especially heavy and asymmetric at high antenna displacement and correspondingly fluctuation poloidal wavenumber. The tail is opposite to the mean frequency shift of the spectrum and presumably caused by drift modes excited in plasma at a low level and rotating in the direction of the ion diamagnetic drift.

Fig. 4 allows us to obtain estimations for the fluctuation poloidal velocity in experiment and in the computation. The estimation of the mean fluctuation poloidal velocity in experiment is given by $v_\theta = \pi f_D / k_\theta \approx 2.1 \pm 0.2$ km/s , whereas the synthetic DR computations result in $v_\theta \approx 2.0 \pm 0.1$ km/s for the fast diagnostics and $v_\theta \approx 2.4 \pm 0.1$ km/s for the full-wave one. The obtained agreement between the measured and computed DR spectra, which are determined by the plasma flows, provides evidences in favor of correct modeling of plasma poloidal rotation and a correct reproduction of the radial electric field behavior in the FT-2 tokamak by the ELMFIRE code.

As it is seen in Fig.5, the mean width of synthetic spectra is systematically smaller than in experiment. However the difference is in the range of only 20 – 30 %. It could be attributed to the contribution of the spectra tails, which are higher in the experiment.

The large backscattering spectrum width seen in Fig.5 is partly associated with strong plasma potential oscillations caused by geodesic acoustic mode (GAM) excited in the FT-2 plasma [5, 6, 21]. These oscillations could be extracted from the DR signal using information on the temporal behavior of the frequency shift of its spectrum [7]. Utilizing 5 μs samples of experimental and synthetic DR signal the following dynamics of the plasma poloidal velocity shown in Fig.6 was obtained. The oscillations in the $v_\theta(t)$ behavior are caused by the GAM. The velocity oscillation amplitudes provided by measurement and fast synthetic diagnostics are close (1.9±0.3 km/s and 1.7±0.2 km/s accordingly). The standard deviation of the velocity fluctuations determined using DR data are also similar: 1.1 km/s is obtained in experiment and 0.9 km/s is given by the fast synthetic diagnostics. The GAM is represented by a line in Fourier spectrum of velocity shown in Fig.7. As it is seen in the figure, the experimental value of the GAM frequency is 40 kHz, whereas the computational value provided by the fast synthetic diagnostics is slightly higher – 45 kHz.

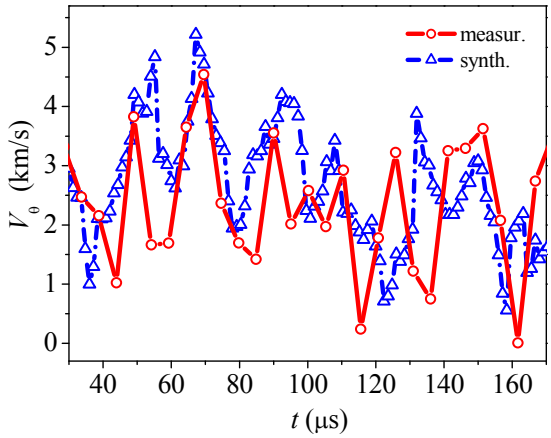

FIG. 6 Poloidal velocity temporal behavior. Solid curve – measured fluctuation velocity; dashed-dotted curve – fluctuation velocity by synthetic diagnostics.

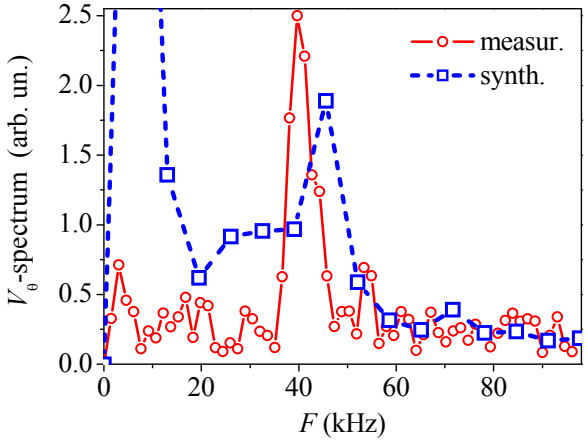

FIG. 7 Power frequency spectra of oscillations shown in Fig.6. Solid curve – measured fluctuation velocity; dotted curve – fluctuation velocity by synthetic diagnostics.

We have also compared the DR signal intensity $\int P_s(f)df_s$ dependence on the vertical antenna displacement, which is expressed in Fig.8 in terms of the poloidal wavenumber of the turbulence. As it is seen in Fig.8, the decrease of the DR signal power with growing fluctuation poloidal wavenumber is substantially faster than in experiment for both synthetic diagnostics. The difference could be attributed to an underestimation of the turbulence poloidal wavenumber spectrum in the intermediate-scale domain $\kappa_\theta \approx 10$ cm^{-1} which occurs in spite of a sufficiently high density of the GK code grid (poloidal cell size 0.06 cm).

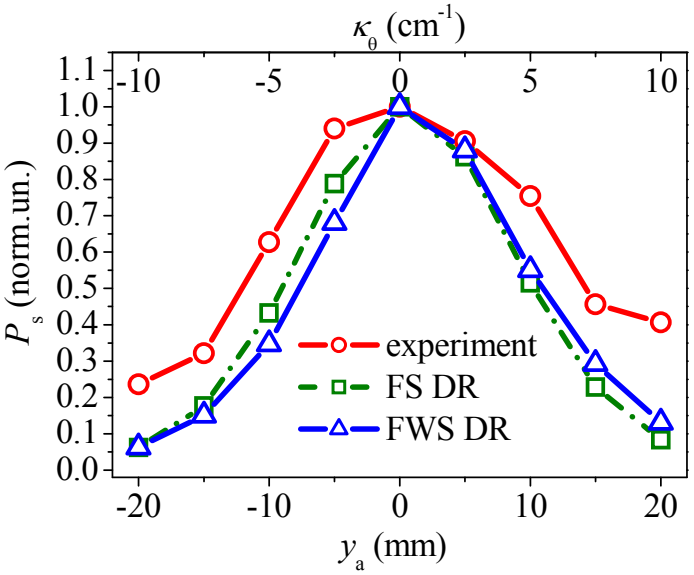

FIG. 8 Dependence of the backscattering power on the fluctuation poloidal wavenumber. Circles –experiment; triangles – fast synthetic DR; squares – full-wave synthetic DR.

5. RCDR CCF COMPARISION

Inspired by a reasonable agreement of the experimental and synthetic DR spectral data we have performed the comparison of the computed and measured RCDR CCFs using the X-mode DR antenna displaced by 2.0 cm from the equatorial plane at the high-field side of the FT-2 tokamak. The corresponding CCFs shown in Fig.9 as functions of the frequency difference in the master and slave channels (a) and of turning point separation (b) appear to be different whereas the density fluctuations two-point CCF for frequency $f = f_s - f_i = 300$ kHz computed in the measurement region based on the GK data and shown in Fig.9b is close to the measured RCDR CCF, as it was mentioned in [15]. The CCF provided by the fast synthetic RD is much wider than the experimental one, whereas the ful-wave synthetic CCF is situated in between, as it is seen in Fig.9a. The slow decay of the CCF provided by fast synthetic diagnostics shown in Fig9a,b is most likely determined by the small-angle-scattering contribution to the DR signal [10], which is not suppressed at the angle of incidence corresponding to y_a =2.0 cm. There are two possible reasons of the drastic difference between the experimental and the fast synthetic RCDR CCFs. The first one is related to nonlinear effects, in particular, the multiple small-angle scattering, or strong probing wave phase modulation, according to theory [12, 22, 23], coming into play with growing turbulence level. The importance of this effect for the DR diagnostics performance was shown recently at ASDEX-upgrade [24]. The second is related to the GK code spatial grid limitations leading to underestimation of the turbulence radial wavenumber spectrum width and thus - to overestimating of the RCDR CCF width.

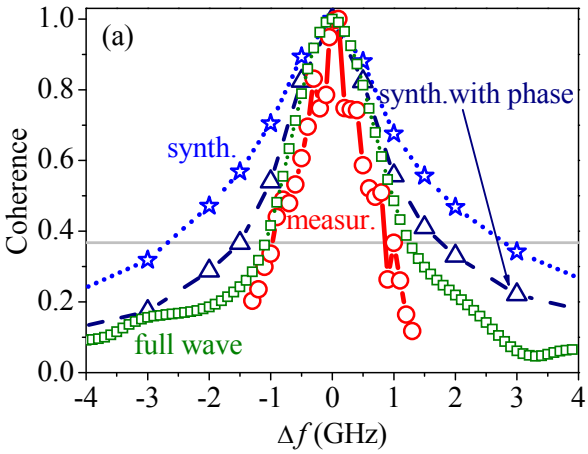

FIG. 9a The RCDR CCF against the channel frequency separation. Stars – fast synthetic DR; squares – full-wave synthetic DR; triangles – fast synthetic DR with phase modulation; circles – experiment.

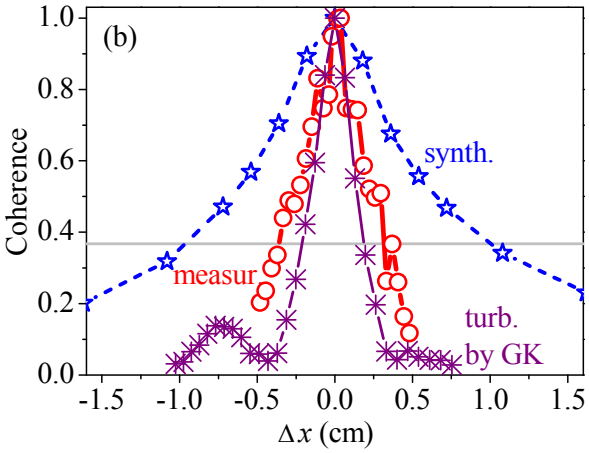

FIG. 9b The RCDR CCF against the turning point radial separation. Stars – fast synthetic DR; circles – experiment; double crosses – turbulence CCF by GK code.

To check the role of nonlinear effects in the FT-2 X-mode RCDR experiment we have computed and measured the random phase perturbation of the backscattered wave and determined its rms. In the computation only the contribution of the long-scale turbulence to the probing and scattered wave phase was taken into account. The calculation was performed along the ray trajectory unperturbed by density fluctuations using the expression [20]

$$\tilde{\varphi}(\omega,t,l) = -\frac{\omega^2}{c^2}\int_0^l \frac{h_X(l')}{k_X(l')}\frac{\tilde{n}(l',t)}{n_c}dl' \qquad (1)$$

where the density fluctuation $\tilde{n}(l,t)$ is provided by the GK computation, whereas the factor $h_X(l,\omega)$, according to [23] is given by expression

$$h_X(l,\omega) = \frac{\left[\omega^2 - 2\omega_{pe}^2(l)\right]\left[\omega^2 - \omega_{ce}^2(l)\right] + \omega_{pe}^4(l)}{\left[\omega^2 - \omega_{pe}^2(l) - \omega_{ce}^2(l)\right]^2} \qquad (2)$$

and $k_X(\omega,l) = \sqrt{\dfrac{\left[\left(\omega+\omega_{ce}(l)\right)\omega - \omega_{pe}^2(l)\right]\left[\left(\omega-\omega_{ce}(l)\right)\omega - \omega_{pe}^2(l)\right]}{\left[\omega^2 - \omega_{pe}^2(l) - \omega_{ce}^2(l)\right]c^2}}$ is the X-mode wavenumber;

Dependencies of the random density fluctuation amplitude and factor $h_X(l,\omega)\omega/k_X c$ on the coordinate along the ray trajectory are shown in Fig.10a for different computation moments.

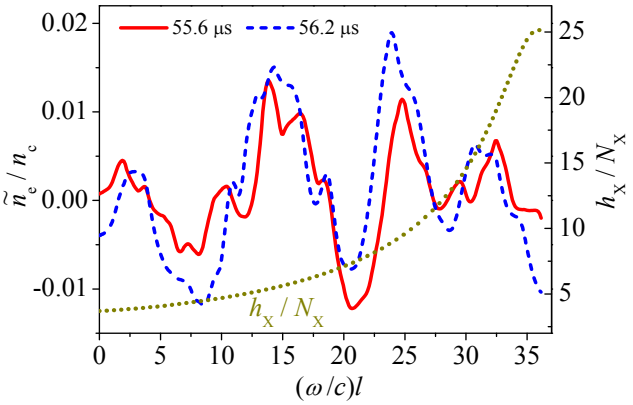

FIG. 10a Density fluctuations (at three different moments of time) and h-factor behavior along the ray trajectory.

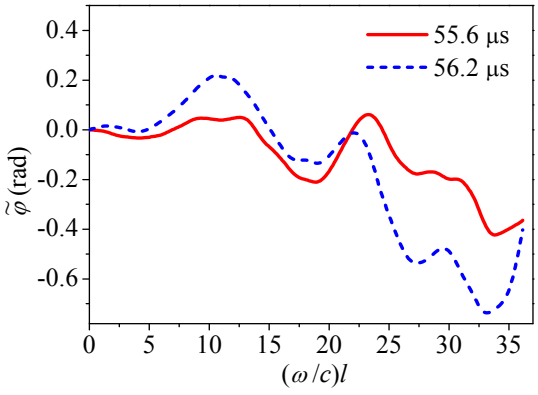

FIG. 10b The phase perturbation variation along the ray trajectory at three different moments of time.

As it is seen in the figure the factor h_X is substantially larger than unity all over the trajectory and increases further when approaching the cut-off surface. This enhancement is associated with a small separation of the cut-off and the UHR layers in our experiment. Due to this effect the phase integral (3) is steeply growing when approaching the turning point l_c, as it is seen in Fig.10b, and gets the value close to π/4.

The temporal behaviour of the computed backscattering signal phase $\tilde{\varphi}(\omega,t,l_c)$ shown in Fig.11 by dashed curve demonstrates variation in the range approximately from $-\pi/2$ to $+\pi/2$, which corresponds to the DR signal substantial phase modulation indicating transition to the nonlinear regime.

The temporal variation of the DR signal phase was also measured experimentally utilizing a quadrature scheme with the intermediate frequency reference signal inversion. The example of the reconstructed phase temporal behaviour is shown in Fig.11 by the solid curve. The interval of the DR signal random phase variation appears to be close to that determined numerically. The standard deviation of the computed DR signal phase there is 0.93, whereas for the measured phase SD it is 1.23. The latter value is close to the computed one and to the level, which indicates the borderline for the DR diagnostics transition into the nonlinear regime of operation. In this parameter domain, strictly speaking, the reciprocity theorem (1) is not applicable. The obtained agreement of the measured and computed DR signal random phase standard deviation and its relatively high value demonstrates importance of the first, based upon nonlinear effects, explanation of the drastic disagreement of the experimental and fast synthetic RCDR diagnostics results. A comparatively low threshold of the X-mode DR transition to the regime nonlinear in the turbulence amplitude is explained by the probing wave strong dispersion.

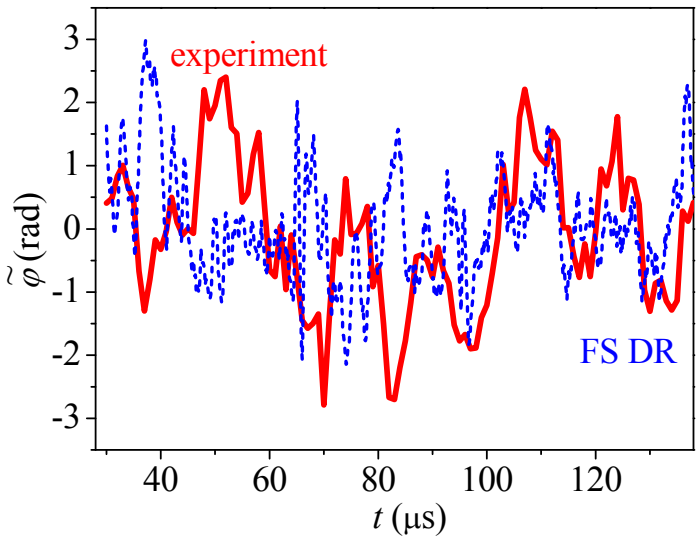

FIG.11 The DR signal phase temporal variation. Fast synthetic signal – dashed line (SD = 0.93); experiment – solid line (SD = 1.23).

In the nonlinear wave propagation and scattering regime the synthetic DR diagnostics should be based upon a full-wave code accounting for the turbulence influence on the probing and scattering wave propagation [25]. Nevertheless an estimation of the multiple small-angle scattering effect onto the RCDR CCF could be obtained just by multiplying the DR signal $A_{s\omega}(t)$ provided by the reciprocity theorem (1) by the phase factor $\exp[i\tilde{\varphi}(\omega,t,l_c)]$ and evaluation of the CCF for the modified signals $A_{s\omega}(t)\exp\left[i\tilde{\varphi}(\omega,t,l_c)\right]$ at different probing frequencies. The corresponding modified fast synthetic DR CCF appears to be close to the CCF provided by the full-wave synthetic diagnostics, as it is seen in Fig.9a, thus confirming this approach based on the natural assumption justified in theory that the backscattering in DR is well localised in the trajectory turning point vicinity [26] whereas the phase modulation is performed by the long-scale fluctuations all over the trajectory [12].

It should be underlined that the CCF provided by the full-wave synthetic diagnostics is very close to the experimental one, thus demonstrating a minor role of the second reason mentioned above, namely, providing an argument in favour of correct description of the turbulence radial wavenumber spectrum by the GK code with the utilized grid. It is necessary to stress that the computational grid cell sizes (0.07cm - radial and 0.06cm – poloidal) are sufficient for adequate description of fluctuations contributing to the DR signal (poloidal wavenumber - 0.4cm) and corresponding to the measured radial correlation length (radial wavelength - 0.7cm). Therefore possibly distortions in numerical description of much smaller scale fluctuations result in underestimation of the measured poloidal scale turbulent fluctuation amplitude by the ELMFIRE code.

6. CONCLUSIONS

Basing on the results of the paper one should conclude that the ELMFIRE code benchmarking against the FT-2 X-mode Doppler reflectometry experimental data utilising the fast linear and full-wave DR synthetic diagnostics have demonstrated a good agreement between the measured and computed DR frequency spectra. For all used incidence angles both the spectra frequency shift and width, and in many cases the spectra form, were similar. The mean fluctuation velocity was close in the DR measurements and in the synthetic diagnostics. The GAM characteristics provided by the measurements and by the synthetic DR appear to be close, as well.

However the variation of the DR signal at growing incidence angles in experiment is slower than predicted by both synthetic diagnostics. This difference could be presumably attributed to the overestimation of the turbulence poloidal wavenumber spectrum decay rate with growing wavenumber due to incorrect modelling in the small-scale domain.

The substantial difference was found also in the decay of the DR signal CCFs with growing frequency shift in the probing wave channels. The quick decrease of the RCDR coherence observed in the experiment and full-wave synthetic diagnostic compared to the fast synthetic RCDR is attributed to the phase modulation of the probing wave in the former two cases due to the long-scale density fluctuations, which is shown to be close to $\pi/4$ both in the specially performed measurements and in the GK modelling. In spite of the fact that this value indicates only the beginning of the transition to the fluctuation reflectometry nonlinear regime, which therefore is not influencing the DR spectra, it already has a strong influence on the RCDR performance. A comparatively low threshold (in density fluctuation RMS and probing trajectory length) of the X-mode DR transition to the regime nonlinear in the turbulence amplitude due to the probing wave strong dispersion should also be mentioned.

ACKNOWLEDGEMENTS

The financial support of the Russian Science Foundation grant 17-12-01110 is acknowledged. The work has been supported by the Academy of Finland grants 278487 and 296853 and 318314. CSC – IT Center for Science is acknowledged for generous allocation of computational resources for this work. The FT-2 tokamak maintenance and M.A. Irzak participation were supported by Ioffe Institute.

REFERENCES

[1] P.H. DIAMOND et al., Plasma Phys. Control. Fusion **47**, R35 (2005).
[2] P.W. TERRY, Reviews of Modern Physics **72**, 109 (2000).
[3] J.A. HEIKKINEN et al., J. Comp. Phys. **227**, 5582 (2008).
[4] Y. SARAZIN et al., Nucl. Fusion 51, 103023 (2011).
[5] S LEERINK et al., Phys. Rev. Lett., **109** 165001, (2012).
[6] E.Z. GUSAKOV, A.B. ALTUKHOV, V.V. BULANIN et al. Plasma Phys. Control. Fusion, **55,** 124034 (2013).
[7] CONWAY A.D., SCOTT B., SCHIRMER J. et al. Plasma Phys. Control. Fusion **47,** 1165 (2005).
[8] HENNEQUIN P, SABOT R, HONORE C et al. Plasma Phys.Control. Fusion **46** B121 (2004).
[9] SCHIRMER J et al. Plasma Phys. Control. Fusion **49** 1019 (2007).
[10] E GUSAKOV, M IRZAK AND A POPOV Plasma Phys. Control. Fusion **56,** 025009 (2014).
[11] E GUSAKOV, M IRZAK, A POPOV et al. Physics of Plasmas **24**, 022119 (2017).
[12] E.Z. GUSAKOV,A.V. SURKOV, A.YU. POPOV, Plasma Phys. Control. Fusion **47,** 959 (2005).
[13] A. B. ALTUKHOV, A. D. GURCHENKO, E. Z. GUSAKOV et.al. Phys. Plasmas **25**, 082305 (2018).
[14] LECHTE C et al. Plasma Phys Control. Fusion **59,** 07500 (2017).
[15] ALTUKHOV A.B., GURCHENKO A.D. et al. Plasma Phys. and Controlled Fusion **58,** 105004 (2016).
[16] T. TAKIZUKA et al., J. Comput. Phys. **25**, 205 (1977).
[17] T.P. KIVINIEMI et al. Plasma Phys. Control. Fusion **56,** 075009, (2014).
[18] S. LEERINK, PhD-thesis, Aalto University http://lib.tkk.fi/Disshttp://lib.tkk.fi/Diss (2012).
[19] A. D. PILIYA, A. YU. POPOV, Plasma Phys. Control. Fusion **44**, 467 (2002).
[20] E.Z. GUSAKOV, V.V. DYACHENKO, M.A. IRZAK et al. Plasma Phys. Control. Fusion 52, 075018 (2010).
[21] A D GURCHENKO, E Z GUSAKOV, A B ALTUKHOV et al. PPCF **55,** 085017 (2013).
[22] E.Z. GUSAKOV, A.YU. POPOV, Plasma Phys. and Control. Fusion, v.44, No 11, p.2327 (2002).
[23] E.Z. GUSAKOV, A.YU. POPOV, Plasma Phys. Control. Fusion **46,** 1393 (2004).
[24] T HAPPEL, T GÖRLER, P HENNEQUIN et al. Plasma Phys. Control. Fusion **59,** 054009 (2017).
[25] C. LECHTE IEEE Transaction on Plasma Science **37**, 6 (2009).
[26] E.Z.GUSAKOV, A. V. SURKOV, Plasma Phys. Control. Fusion, v.46 p.1143 (2004).